

Cite this: *J. Mater. Chem. C*, 2022,
10, 11855Received 11th July 2022,
Accepted 10th August 2022

DOI: 10.1039/d2tc02909j

rsc.li/materials-c

Multiple resonance thermally activated delayed
fluorescence enhanced by halogen atoms†Youngnam Lee  and Jong-In Hong *

We synthesized halogen-substituted multiple-resonance (MR) thermally activated delayed fluorescence emitters, namely 2,12-dichloro-*N,N*,5,9-tetrakis(4-chlorophenyl)-5,9-dihydro-5,9-diaza-13*b*-boranaphtho[3,2,1-*de*]anthracen-7-amine (Cl-MR) and 2,12-dibromo-*N,N*,5,9-tetrakis(4-bromophenyl)-5,9-dihydro-5,9-diaza-13*b*-boranaphtho[3,2,1-*de*]anthracen-7-amine (Br-MR). Cl-MR and Br-MR exhibited a decreased delayed fluorescence lifetime and an enhanced reverse intersystem crossing rate without any changes in ΔE_{ST} and orbital distribution compared with a non-halogenated MR emitter. Cl-MR exhibited a high photoluminescence quantum yield (PLQY) of 85% and external quantum efficiency (EQE) of 17%; however, Br-MR did not exhibit any enhancement in the PLQY and EQE. The different performances of Cl-MR and Br-MR were rationalized by analysing the rate constants of the excited states and bond dissociation energies of the carbon-halogen bonds.

1. Introduction

Recently, a number of studies have been conducted to develop organic light-emitting diode (OLED) emitters using thermally activated delayed fluorescence (TADF).^{1–3} TADF emitters typically consist of twisted electron donor-acceptor structures to separate the highest occupied molecular orbital (HOMO) and lowest unoccupied molecular orbital (LUMO). Consequently, the energy difference between the singlet and triplet states (ΔE_{ST}) could be sufficiently small to reverse the intersystem crossing (ISC) between the singlet and triplet states. Thus, triplet states can also participate in the emission, as delayed fluorescence and 100% internal quantum efficiency can be achieved. Based on this concept, several devices involving high external quantum efficiency (EQE) of red, green, and blue emitters have been reported.^{4–6} However, because twisted TADF

structures exhibit strong charge transfer emission and possess high reorganization energy,⁷ OLED fabrication leads to a wide full width at half maximum (FWHM).

Hatakeyama *et al.* solved the problem of a wide FWHM by introducing an electron-withdrawing boron and an electron-donating nitrogen into a fused ring.³ Controlling the positions of the boron and nitrogen atoms causes a difference in the electron distribution along the *ortho*, *meta*, and *para* positions relative to those atoms. This results in the separation of the HOMO and LUMO, similar to the distorted TADF structures, thus emitting a TADF emission. This phenomenon is known as multiple-resonance thermally activated delayed fluorescence (MR-TADF). In addition, the fused ring structure provides structural rigidity, leading to enhanced photoluminescence quantum yields (PLQYs) and reduced FWHM values.

The delayed fluorescence lifetime of a twisted TADF emitter is short because the HOMO and LUMO are almost entirely separated.⁸ However, the ΔE_{ST} values of MR-TADF molecules are relatively large compared to those of twisted TADF molecules because their HOMO and LUMO are not completely separated.⁹ Therefore, MR-TADF emitters typically have a small contribution from a delayed component to the total PLQY and a long delayed fluorescence lifetime. Recently, sensitizers were introduced to resolve the long delayed fluorescence lifetime of MR-TADF.^{10,11} However, with the introduction of sensitizer, the electronic interactions between the host, sensitizer, and MR-TADF emitter must be considered in a complicated manner.¹² Therefore, these intrinsic problems of MR-TADF emitters can be overcome by reducing the delayed lifetime of the MR-TADF molecule itself.

The interactions between the singlet and triplet states can be expressed by eqn (1) as follows:

$$\lambda \propto H_{SO}/\Delta E_{ST} \quad (1)$$

The first-order mixing coefficient (λ) between the singlet and triplet states is proportional to the spin-orbit interaction (H_{SO}) and inversely proportional to ΔE_{ST} .¹³ Twisted TADF molecules can enhance λ by lowering ΔE_{ST} , but because MR-TADF emitters

Department of Chemistry, Seoul National University, Seoul 08826, Republic of Korea. E-mail: jihong@snu.ac.kr

† Electronic supplementary information (ESI) available. See DOI: <https://doi.org/10.1039/d2tc02909j>

have some overlap of the HOMO and LUMO, they cannot significantly reduce the ΔE_{ST} . However, λ can be increased by increasing the H_{SO} despite the large ΔE_{ST} . When a heavy atom is introduced, the orbital and spin angular momentum are mixed, thus increasing the H_{SO} ; this is called the heavy-atom effect. The heavy-atom effect can be introduced not only by transition metals such as Ir or Pt but also by halogen atoms such as chlorine and bromine.^{14–18}

With the introduction of halogens into twisted TADF emitters, the performance of OLED devices improved in some cases.^{16–18} However, a negative effect of halogens was observed when halogens were introduced into the TADF emitters with a large rate constant of reverse intersystem crossing (k_{RISC}).¹⁶ These molecules did not emit fluorescence from the excited state because the rate constants of intersystem crossing (k_{ISC}) ($\sim 10^8$) and k_{RISC} ($\sim 10^7$) were larger than the rate constant of radiative decay (k_r^2) ($\sim 10^6$). However, when halogens were introduced to twisted TADF molecules with a small k_{RISC} , the PLQY, EQE, and roll-off were improved.¹⁸ MR-TADF molecules have a large k_r^2 of 10^7 – 10^8 but a very small k_{RISC} of 10^4 . Recently, the k_{RISC} values of MR-TADF emitters were drastically enhanced by introducing heavy chalcogens.^{19–21} We also expected that the small k_{RISC} problem of MR-TADF emitters could be resolved by introducing halogens. Herein, we report the first case of improving the TADF performance by introducing halogens into an MR-TADF molecule.

We have designed 2,12-dichloro-*N,N*,5,9-tetrakis(4-chlorophenyl)-5,9-dihydro-5,9-diaza-13*b*-boranaphtho[3,2,1-*de*]anthracen-7-amine (Cl-MR) and 2,12-dibromo-*N,N*,5,9-tetrakis(4-bromophenyl)-5,9-dihydro-5,9-diaza-13*b*-boranaphtho[3,2,1-*de*]anthracen-7-amine (Br-MR), in which six Cl and Br atoms were substituted for six peripheral H atoms at the *para* positions of three N atoms of an *N,N*,5,9-tetraphenyl-5,9-dihydro-5,9-diaza-13*b*-boranaphtho[3,2,1-*de*]anthracen-7-amine (MR) emitter, respectively. The syntheses of Cl-MR and Br-MR were simple, even in the presence of six halogen atoms, *via* one-pot borylation. Density functional theory (DFT) and time-dependent density functional theory (TD-DFT) calculations revealed enhanced spin-orbit coupling in both Cl-MR and Br-MR. Experimental observation through photoluminescence (PL) and transient PL studies confirmed that halogenated MR emitters efficiently used triplet states in both the solution and film states. In particular, Cl-MR exhibited an improved PLQY (85%) compared with MR (75%) and an EQE of 17%. However, despite the significantly reduced delayed lifetime of Br-MR, its PLQY and EQE did not improve. This was rationalized through the analysis of kinetic rates and calculations of bond dissociation energy (BDE).

2. Results and discussion

2.1 Calculations

DFT and TD-DFT calculations were performed to make theoretical predictions of the geometries, orbital distributions, spin-orbit coupling constants, and energies of the excited states. The geometries in the ground state were optimized with the B3LYP functional and the 6-31G(d) basis set using Gaussian 09 software. Calculations for Br-MR were performed using the B3LYP functional and

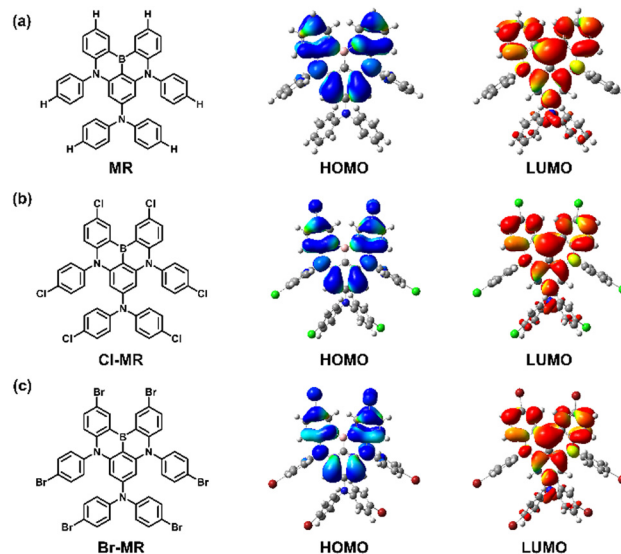


Fig. 1 Molecular structures and frontier orbitals (blue: HOMO, red: LUMO). (a) MR, (b) Cl-MR, and (c) Br-MR.

LANL2DZ basis sets. The spin-orbit coupling constants were calculated using TD-DFT with the B3LYP/G functional and the def2-SVP basis set in ORCA 5.0.1 software. The calculated results are shown in Fig. 1 and summarized in Table 1. Because MR, Cl-MR, and Br-MR are all MR-TADF molecules, they exhibit different orbital distributions between the HOMO and LUMO along the *ortho*, *meta*, and *para* positions. The substitution of halogen atoms did not cause any changes in the frontier orbitals. To examine the effect of halogen atoms in the excited state, natural transition orbital (NTO) calculations were also performed by employing the B3LYP functional and the 6-31G(d) basis set using Gaussian 09 (Fig. S1–S3, ESI†). The halogen atoms also did not cause any changes in NTO 1, 2, and 3. Therefore, even if halogens are introduced, there is no change in the PL mechanism.

When an electron-donating group (EDG) is introduced, E_{gap} decreases while the HOMO and LUMO increase; however, in the case of the electron-withdrawing group (EWG), E_{gap} increases while the HOMO and LUMO decrease.^{22,23} Unlike typical EDGs or EWGs, a halogen element can act as both EDG and EWG. The halogen element can act as an EDG because of the non-bonding orbital on the halogen or as an EWG owing to its electronegativity. Therefore, when halogen atoms are introduced, E_{gap} may decrease, whereas both HOMO and LUMO decrease. This tendency was confirmed using DFT calculations. Changes in H_{SO} owing to the substitution by halogen elements were confirmed using TD-DFT calculations. With the introduction of Cl and Br, H_{SO} sequentially increased from no substitution to Cl and Br substitution *via* the heavy-atom effect. Therefore, it is expected that Cl and Br can enhance TADF emissions by accelerating the singlet–triplet interactions.

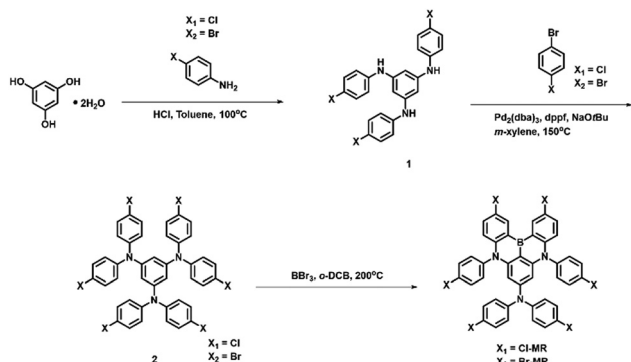
2.2 Synthesis

Cl-MR and Br-MR were synthesized as shown in Scheme 1. First, compound **1** was prepared by dehydration of

Table 1 Calculated data

| Compound | HOMO [eV] | LUMO [eV] | E_{gap}^a [eV] | S_1^b [eV] | T_1^c [eV] | T_2^d [eV] | $\langle S_1 H_{\text{SO}} T_1 \rangle^e$ [cm^{-1}] | $\langle S_1 H_{\text{SO}} T_2 \rangle^f$ [cm^{-1}] |
|----------|-----------|-----------|-------------------------|--------------|--------------|--------------|--|--|
| MR | 4.76 | 1.08 | 3.68 | 3.145 | 2.678 | 2.927 | 0.06 | 0.19 |
| Cl-MR | 5.33 | 1.75 | 3.58 | 3.043 | 2.581 | 2.857 | 0.06 | 0.68 |
| Br-MR | 5.42 | 1.84 | 3.58 | 3.052 | 2.599 | 2.864 | 0.19 | 2.21 |

^a Energy gap between the HOMO and LUMO. ^b Energy of the 1st singlet excited state. ^c Energy of the 1st triplet excited state. ^d Energy of the 2nd triplet excited state. ^e Spin-orbit coupling constant between the S_1 and T_1 . ^f Spin-orbit coupling constant between the S_1 and T_2 .



Scheme 1 Synthetic routes of Cl-MR and Br-MR.

phloroglucinol and 4-halogenated aniline using an acid catalyst.²⁴ Next, compound 2 was synthesized by reacting 1 with aryl bromide *via* the Buchwald Hartwig reaction using the 1,1'-bis(diphenylphosphino)ferrocene (dppf) ligand. Finally, Cl-MR and Br-MR were synthesized using BBr_3 *via* one-pot borylation at 200 °C in *ortho*-dichlorobenzene (*o*-DCB). MR-TADF molecules with a fused ring structure are typically constructed through selective borylation *via* a lithium-halogen exchange reaction.³ However, in the case of halogenated MR-TADF, it is challenging to selectively perform borylation through lithium-halogen exchange because of the presence of pre-existing halogens. DFT calculations (B3LYP/6-31G(d)) were performed to predict the orbital distributions of 2-Cl and 2-Br. Electrons in the HOMOs of 2-Cl and 2-Br are mainly concentrated at the *ortho*-position of nitrogen (Fig. S4, ESI[†]). Therefore, we were able to selectively perform borylation in a one-pot reaction without a lithium-halogen exchange reaction. The new compounds were purified by column chromatography, recrystallisation, and vacuum thermal sublimation. Cl-MR and Br-MR were fully characterized by proton nuclear magnetic resonance (¹H-NMR), carbon nuclear magnetic resonance (¹³C-NMR), and high-resolution mass spectrometry (HR-MS), and elemental analysis (EA).

2.3 Photophysical properties

Photophysical and electrochemical properties were evaluated using ultraviolet-visible (UV-vis) absorption, cyclic voltammetry (CV), photoluminescence (PL), and time-correlated single-photon counting (TCSPC) experiments. The photophysical properties of the emitters in the solution and film states are shown in Fig. 2 and 3 and summarized in Tables 2 and 3. MR exhibited UV absorption at 430 nm, and Cl-MR and Br-MR at

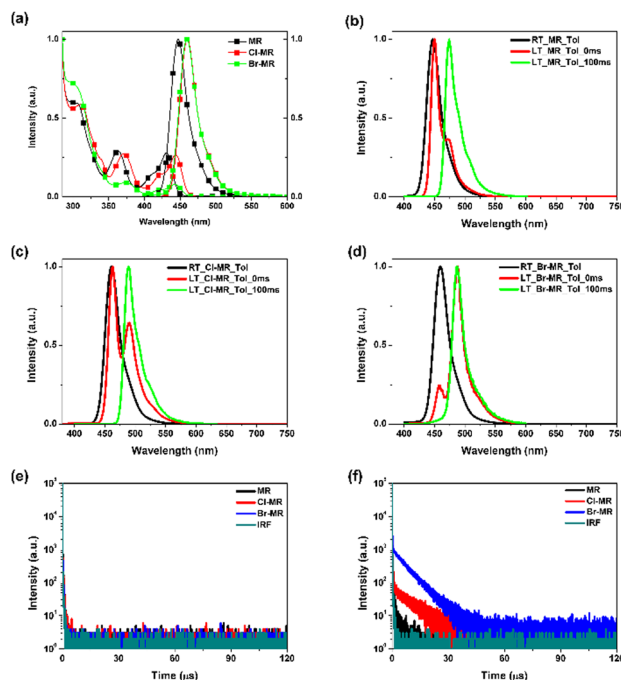


Fig. 2 Photophysical properties in toluene (10^{-5} M) solution. (a) UV-vis and PL, (b) fluorescence and phosphorescence spectra of MR, (c) fluorescence and phosphorescence spectra of Cl-MR, (d) fluorescence and phosphorescence spectra of Br-MR, (e) transient PL in aerated toluene solution, and (f) transient PL in toluene solution after argon bubbling.

443 nm, which correspond to the HOMO–LUMO transition. The HOMO levels of MR, Cl-MR, and Br-MR were calculated using CV measurements. The LUMO energies were calculated from CV and UV-vis measurements. The HOMO and LUMO of MR were at 5.09 and 2.32 eV, respectively, whereas Cl-MR and Br-MR exhibited a HOMO at 5.28 eV and a LUMO at 2.60 eV. As observed from the DFT calculations, both the HOMO and LUMO decreased, and E_{gap} also decreased under the influence of halogen atoms. As E_{gap} reduced, the maximum emission wavelength was red-shifted in Cl-MR (460 nm) and Br-MR (460 nm) compared to that in MR (447 nm). However, no changes were observed in the spectral shape. The FWHM values were the same for MR, Cl-MR, and Br-MR (27 nm in the solution and 36 nm in the film). This result can be attributed to the same emission mechanism for MR, Cl-MR, and Br-MR, as shown in the NTO calculations.

To obtain the ΔE_{ST} values for MR, Cl-MR, and Br-MR, their PL spectra in toluene were examined at room temperature (RT) and 77 K (Fig. 2). All three compounds exhibited fluorescence

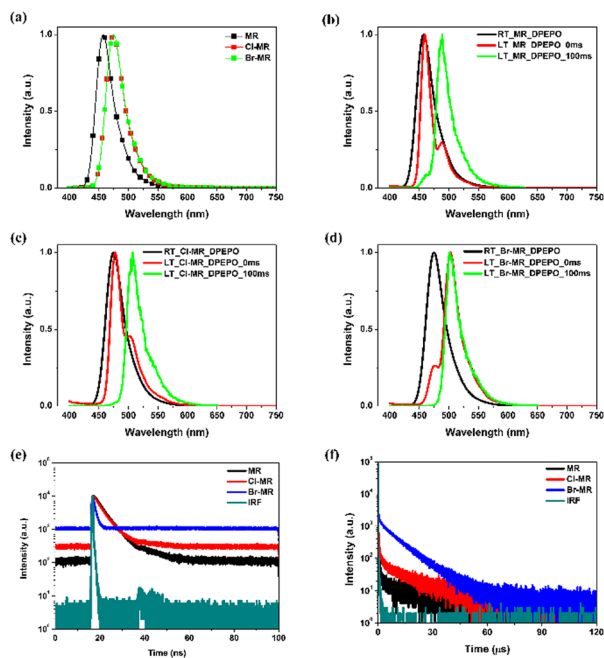


Fig. 3 Photophysical properties of the 10 wt% doped films in the DPEPO host. (a) PL spectra, (b) fluorescence and phosphorescence spectra of MR, (c) fluorescence and phosphorescence spectra of Cl-MR, (d) fluorescence and phosphorescence spectra of Br-MR, (e) transient PL of PicoHarp mode, and (f) transient PL of NanoHarp mode.

only at RT and phosphorescence at 77 K with a 100 ms delay. MR, Cl-MR, and Br-MR exhibited the same ΔE_{ST} values, indicating that the halogens had no effect on ΔE_{ST} . However, the PL spectra measured without delay at 77 K in toluene exhibited different phosphorescence and fluorescence ratios. In the case of typical TADF emitters, the H_{SO} was low based on the spin selection rule, and thus fluorescence is predominant at low

temperatures with a 0 ms delay.²⁵ However, owing to the heavy-atom effect, relative intensity of phosphorescence *versus* fluorescence increased in the order of MR, Cl-MR, and Br-MR, parallel with the atomic size. That is, the singlet–triplet interaction was the strongest in Br-MR despite having the same ΔE_{ST} . This tendency was also observed through TCSPC. All three compounds exhibited fluorescence without TADF emissions in an aerated toluene solution. However, after bubbling for 10 min using argon gas, all three materials exhibited TADF emission, but the ratio of TADF emission increased in the order of MR, Cl-MR, and Br-MR. Consequently, low-temperature PL and TCSPC experiments verified the effect of the halogen atoms in solution states.

To confirm the photophysical properties of the films, 10 wt% doped films with a thickness of 50 nm were deposited on quartz using a bis [2-(diphenylphosphino)phenyl] ether oxide (DPEPO) host. To confine all the triplets, DPEPO with high triplet energy (3.0 eV) was used.²⁶ The HOMO and LUMO of DPEPO (6.5 and 2.5 eV, respectively) were also properly aligned with MR, Cl-MR, and Br-MR.²⁷ At RT, the emission wavelength of the doped films was slightly red-shifted, and the FWHM increased by 9 nm because of the polarity of DPEPO (Table 2). Because of the different E_{gap} values of MR and Cl-MR/Br-MR, the emission wavelengths of Cl-MR and Br-MR were also red-shifted compared to those of MR, but the shape and FWHM of the spectra were the same. As in the toluene solution, the PL spectra of the doped films at RT and 77 K with a 100 ms delay exhibited only fluorescence and phosphorescence, respectively (Fig. 3). However, at 77 K with a 0 ms delay, the ratio of phosphorescence to fluorescence increased in the order of MR, Cl-MR, and Br-MR, as in the toluene solution states. The singlet and triplet interactions in the film state also increased in the same order as that in the solution state.

The effect of the halogens was also confirmed through TCSPC using the doped films. The rate constants were

Table 2 Photophysical and electrochemical properties of MR series

| Compound | $\lambda_{max}^{a/b}$ [nm] | FWHM ^{a/b} [nm] | HOMO ^c [eV] | LUMO ^d [eV] | E_{gap}^e [eV] | S_1^f [eV] | T_1^g [eV] | ΔE_{ST}^h [eV] | Φ^{bi} [%] | Φ_{PF}^{bj} [%] | Φ_{DF}^{bk} [%] |
|----------|----------------------------|--------------------------|------------------------|------------------------|------------------|--------------|--------------|------------------------|-----------------|----------------------|----------------------|
| MR | 447/456 | 27/36 | 5.09 | 2.32 | 2.77 | 2.85/2.80 | 2.71/2.67 | 0.14/0.13 | 75 | 70 | 5 |
| Cl-MR | 460/474 | 27/36 | 5.28 | 2.59 | 2.69 | 2.77/2.71 | 2.63/2.58 | 0.14/0.13 | 85 | 51 | 34 |
| Br-MR | 460/474 | 27/36 | 5.28 | 2.59 | 2.69 | 2.79/2.71 | 2.67/2.59 | 0.14/0.13 | 76 | 13 | 63 |

^a Measured in toluene solution (10^{-5} M). ^b Measured in 10 wt% doped films with the DPEPO host. ^c Estimated from the onset potentials in CV experiments. ^d HOMO + optical energy gap. ^e Optical energy gap. ^f Energy of the 1st singlet state. ^g Energy of the 1st triplet state. ^h Energy difference between the S_1 and T_1 . ⁱ Absolute PLQY. ^j PLQY of prompt fluorescence. ^k PLQY of delayed fluorescence.

Table 3 Lifetimes and rate constants of MR series

| Compound | τ_{PF}^a (ns) | τ_{DF}^b (μ s) | k_r^c ($\times 10^8$) | k_{DF}^d ($\times 10^4$) | k_{IC}^e ($\times 10^7$) | k_{ISC}^f ($\times 10^7$) | k_{RISC}^g ($\times 10^4$) | Φ_r^{sh} (%) | Φ_{IC}^i (%) | Φ_{ISC}^j (%) | $\Phi_r^s \cdot \Phi_{ISC}$ (%) | $\Phi_{IC} \cdot \Phi_{ISC}$ (%) | $\Phi_{ISC} \cdot \Phi_{ISC}$ (%) |
|----------|--------------------|--------------------------|---------------------------|------------------------------|------------------------------|-------------------------------|--------------------------------|-------------------|-------------------|--------------------|---------------------------------|----------------------------------|-----------------------------------|
| MR | 4.6 | 39 | 1.5 | 2.6 | 5.0 | 1.6 | 2.8 | 70 | 23 | 7 | 5 | 1.7 | 0.55 |
| Cl-MR | 4.1 | 17 | 1.2 | 5.8 | 2.2 | 9.8 | 9.8 | 51 | 9 | 40 | 20 | 3.6 | 16 |
| Br-MR | 1.0 | 9.9 | 1.3 | 10 | 4.1 | 83 | 59 | 13 | 4 | 83 | 11 | 3.4 | 69 |

^a Lifetime of prompt fluorescence. ^b Lifetime of delayed fluorescence. ^c Rate constant of radiative decay. ^d Rate constant of delayed fluorescence. ^e Rate constant of internal conversion. ^f Rate constant of intersystem crossing. ^g Rate constant of reverse intersystem crossing. ^h $k_r^s / (k_r^s + k_{IC} + k_{ISC})$. ⁱ $k_{IC} / (k_r^s + k_{IC} + k_{ISC})$. ^j $k_{ISC} / (k_r^s + k_{IC} + k_{ISC})$.

calculated using PLQYs and the lifetimes of prompt and delayed fluorescence (Table 3).^{28,29} First, the lifetime of the prompt component decreased in the order of MR, Cl-MR, and Br-MR (Fig. 3e). Consequently, it was confirmed *via* the Pico-Harp mode that k_{ISC} increased in the order of MR, Cl-MR, and Br-MR owing to the heavy-atom effect. In addition, it was possible to confirm a gradual increase in the PLQY of the delayed fluorescence (Φ_{TADF}) and a decrease in the delayed lifetime (τ_{DF}) through the NanoHarp mode in the order of MR, Cl-MR, and Br-MR (Fig. 3f). However, Br-MR did not exhibit any significant improvement in PLQY compared to MR, despite the increased PLQY of the delayed fluorescence and the decreased lifetime of the delayed component. The reason for this could be analysed by calculating the rate constants of the excited states. Because k_{RISC} is higher than the rate constant of phosphorescence (k_{T}) and non-radiative decay in the triplet state (k_{nr}^{T}), Φ_{RISC} was assumed to be 1.²⁸ In the case of Cl-MR, the probabilities of all the processes occurring from the singlet excited state repopulated from T_1 were as follows: radiative decay was 20%, internal conversion (IC) was 3.6%, and return to T_1 was 16%. In the case of Br-MR, the probabilities of the singlet excited state behavior returning from T_1 were as follows: the radiative decay was 11%, IC was 3.4%, and return to T_1 was 69%. That is, $\Phi_{\text{r}}^{\text{S}} \cdot \Phi_{\text{ISC}}$, $\Phi_{\text{IC}} \cdot \Phi_{\text{ISC}}$, and $\Phi_{\text{ISC}} \cdot \Phi_{\text{ISC}}$ of Cl-MR increased by 4, 2.1, and 29 times compared to MR, respectively. In the case of Br-MR, $\Phi_{\text{r}}^{\text{S}} \cdot \Phi_{\text{ISC}}$, $\Phi_{\text{IC}} \cdot \Phi_{\text{ISC}}$, and $\Phi_{\text{ISC}} \cdot \Phi_{\text{ISC}}$ increased by 2.2, 2, and 125 times compared to MR, respectively. That is, in the case of Br-MR, the excited states did not emit light because of the excessively high ISC and RISC, but rather remained in the excited state. However, in the case of Cl-MR, the PLQY can be further improved by 10% compared to that of MR, owing to the balanced increase in kinetic rates.

2.4 Thermal properties

Thermogravimetric analysis (TGA) and differential scanning calorimetry (DSC) were used to evaluate the thermal stability of the three emitters (Fig. S6, ESI†). The evaluation was carried out using DSC Q10 and TGA Q50 at a heating rate of $10\text{ }^{\circ}\text{C min}^{-1}$ in a nitrogen atmosphere. MR, Cl-MR, and Br-MR did not exhibit glass transition temperatures (T_{g}) from 0 to $250\text{ }^{\circ}\text{C}$. Cl-MR and Br-MR exhibited higher thermal decomposition temperatures (T_{d}) at 450 and $420\text{ }^{\circ}\text{C}$, respectively, compared to MR ($384\text{ }^{\circ}\text{C}$), which indicates that halogen-containing MR exhibited excellent thermal stability.

2.5 Device properties

To confirm the OLED characteristics, the device was constructed as follows: indium tin oxide (ITO) (70 nm)/*N,N'*-bis(naphthalen-1-yl)-*N,N'*-bis(phenyl)benzidine (NPB, 80 nm)/tris(4-carbazoyl-9-ylphenyl)amine (TCTA, 20 nm)/1,3-di(9*H*-carbazol-9-yl)benzene (mCP, 30 nm)/DPEPO: emitter (10 wt%, 20 nm)/2,2',2''-(1,3,5-benzinetriyl)-tris(1-phenyl-1*H*-benzimidazole) (TPBi, 30 nm)/LiF (1 nm)/Al (100 nm). The device data are presented in Fig. 4 and summarized in Table 4. The Br-MR doping concentration was set at 20% because of its extremely low luminance. MR exhibited an EQE of 16% and Commission Internationale de l'Eclairage (CIE)

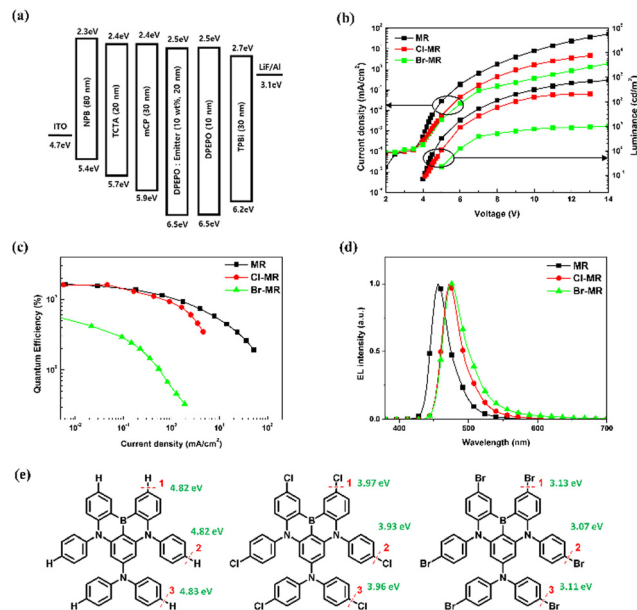


Fig. 4 (a) Optimized device structure of MR series, (b) voltage–current density (V – J) and voltage–luminance (V – L) graph, (c) external quantum efficiency–current density (EQE– J) graph, (d) emission spectra at 10 V, and (e) molecular structures and bond dissociation energies of MR series.

coordinates of (0.14, 0.08). Cl-MR exhibited an EQE of 17% and CIE coordinates of (0.12, 0.19). In particular, the improved EQE of the OLEDs based on Cl-MR was due to more efficient triplet harvesting, as shown by the theoretical calculations and photo-physical studies. However, OLEDs using Br-MR exhibited an extremely low EQE, and the luminance gradually decreased over time, making it difficult to measure. Because OLEDs based on MR, Cl-MR, and Br-MR emitters were all manufactured with the same device structure, the poor device performance can be inferred from the Br-MR itself.

The BDEs of the carbon–halogen bond were employed to understand the low EQE of Br-MR, as it was significantly smaller than those of MR and Cl-MR (Fig. 4e). BDEs were calculated by enthalpy changes using the optimized structures which undergo homolytic bond cleavage of the carbon–halogen bond (Fig. S7–S9 and Tables S1–S3, ESI†). The BDE of the C–H bond in MR was approximately 4.8 eV at all three positions. The BDE of the C–Cl bond in Cl-MR was approximately 3.9 eV, and that of the C–Br bond in Br-MR was approximately 3.1 eV at all three positions (Fig. 4e). The BDE of the C–Br bond in Br-MR was not significantly different from that of S_1 (Table 2) when compared with MR and Cl-MR. Thus, when a voltage of 5 V or more is applied, the accumulated high-energy excitons may affect the bond dissociation of the C–Br bond. Therefore, the OLED pixels would not be emissive as the voltage increased, and it was difficult to measure the OLED performance of the Br-MR-based devices.

In the case of Cl-MR, the BDE of the C–Cl bond is higher than that of Br-MR, but lower than that of MR. The delayed fluorescence lifetime of Cl-MR is shorter than that of MR, and its PLQY is higher than that of MR, but the efficiency roll-off

Table 4 OLED properties and calculated BDE of MR series

| Compound | V_{on}^a (V) | λ_{max}^b (nm) | FWHM ^c (nm) | EQE _{max} ^d (%) | L_{max}^e (cd m ⁻²) | CIE ^f (x, y) | BDE-1 ^g (eV) | BDE-2 ^h (eV) | BDE-3 ⁱ (eV) |
|----------|-----------------------|-------------------------------|------------------------|-------------------------------------|--|-------------------------|-------------------------|-------------------------|-------------------------|
| MR | 4.0 | 456 | 30 | 16 | 732 | 0.14, 0.08 | 4.82 | 4.82 | 4.83 |
| Cl-MR | 4.2 | 472 | 30 | 17 | 209 | 0.12, 0.19 | 3.97 | 3.93 | 3.96 |
| Br-MR | 5.0 | 476 | 39 | 4.2 | 10.3 | 0.14, 0.25 | 3.13 | 3.07 | 3.11 |

^a Turn-on voltage. ^b Emission wavelength at 100 cd m⁻². ^c Full width at half maximum. ^d Maximum EQE at 1 cd m⁻¹. ^e Maximum luminance. ^f CIE 1931 colour coordinates. ^g Bond dissociation energy of the 1st position. ^h Bond dissociation energy of the 2nd position. ⁱ Bond dissociation energy of the 3rd position.

was severe, and the maximum luminance was low. Because the EQE_{max} of Cl-MR at low voltages is higher than that of MR, the triplet must be effectively used compared to MR at low current densities. However, as the voltage increased, the exciton energies increased and are thus close to the BDE, affecting the C–Cl bond, which is more easily dissociated than the C–H bond. It is known that the roll-off of TADF-based OLED devices can be reduced by enhancing k_{RISC} .^{30,31} However, although k_{RISC} was significantly increased by the introduction of halogen atoms, the roll-off and device stability were poor. This suggests that to improve the EQE and roll-off, along with enhancing k_{RISC} , the stability of the emitters should also be considered.

3. Conclusions

We introduced heavy Cl and Br atoms to enhance the k_{RISC} of MR-TADF emitters. The orbital and spin angular momentum were mixed by the heavy atom so that both the solution and the film utilized the triplet states more efficiently than the MR without halogen atoms. Cl-MR exhibited a PLQY of 85% and an EQE of 17%. However, Br-MR did not exhibit any significant improvement in PLQY and EQE, despite the short lifetime of the delayed fluorescence compared to MR. Analysis of the rate constants confirmed the importance of balancing the kinetic rate constants in the singlet and triplet states and shortening the lifetime of the delayed component. In addition, BDE analysis revealed that the weak carbon–halogen bond resulted in the deterioration of the devices, leading to decreased EQEs. Our study suggests that the introduction of a halogen atom could reduce the lifetime of delayed components; however other factors, such as the stability of emitters, must also be considered in the development of MR-TADF emitters.

Conflicts of interest

The authors declare no conflict of interest.

Acknowledgements

This work was supported by the NRF grant funded by the Korea Government (MSIT) (No. 2021R1A2C2009088).

Notes and references

1 H. Uoyama, K. Goushi, K. Shizu, H. Nomura and C. Adachi, *Nature*, 2012, **492**, 234–238.

- D. H. Ahn, S. W. Kim, H. Lee, I. J. Ko, D. Karthik, J. Y. Lee and J. H. Kwon, *Nat. Photonics*, 2019, **13**, 540–546.
- T. Hatakeyama, K. Shiren, K. Nakajima, S. Nomura, S. Nakatsuka, K. Kinoshita, J. Ni, Y. Ono and T. Ikuta, *Adv. Mat.*, 2016, **28**, 2777–2781.
- Y. Lee and J.-I. Hong, *Adv. Opt. Mater.*, 2021, **9**, 2100406.
- J.-X. Chen, K. Wang, C.-J. Zheng, M. Zhang, Y.-Z. Shi, S.-L. Tao, H. Lin, W. Liu, W.-W. Tao, X.-M. Ou and X.-H. Zhang, *Adv. Sci.*, 2018, **5**, 1800436.
- T.-L. Wu, M.-J. Huang, C.-C. Lin, P.-Y. Huang, T.-Y. Chou, R.-W. Chen-Cheng, H.-W. Lin, R.-S. Liu and C.-H. Cheng, *Nat. Photonics*, 2018, **12**, 235–240.
- A. Pershin, D. Hall, V. Lemaur, J.-C. Sancho-Garcia, L. Muccioli, E. Zysman-Colman, D. Beljonne and Y. Olivier, *Nat. Commun.*, 2019, **10**, 597.
- J. U. Kim, I. S. Park, C.-Y. Chan, M. Tanaka, Y. Tsuchiya, H. Nakanotani and C. Adachi, *Nat. Commun.*, 2020, **11**, 1765.
- S. Oda, W. Kumano, T. Hama, R. Kawasumi, K. Yoshiura and T. Hatakeyama, *Angew. Chem., Int. Ed.*, 2021, **60**, 2882–2886.
- S. O. Jeon, K. H. Lee, J. S. Kim, S.-G. Ihn, Y. S. Chung, J. W. Kim, H. Lee, S. Kim, H. Choi and J. Y. Lee, *Nat. Photonics*, 2021, **15**, 208–215.
- C.-Y. Chan, M. Tanaka, Y.-T. Lee, Y.-W. Wong, H. Nakanotani, T. Hatakeyama and C. Adachi, *Nat. Photonics*, 2021, **15**, 203–207.
- Y. Wang, K. Di, Y. Duan, R. Guo, L. Lian, W. Zhang and L. Wang, *Chem. Eng. J.*, 2021, 133221.
- M. Y. Wong and E. Zysman-Colman, *Adv. Mat.*, 2017, **29**, 1605444.
- Z.-G. Wu, Y.-M. Jing, G.-Z. Lu, J. Zhou, Y.-X. Zheng, L. Zhou, Y. Wang and Y. Pan, *Sci. Rep.*, 2016, **6**, 38478.
- C. Cebrián and M. Mauro, *Beilstein J. Org. Chem.*, 2018, **14**, 1459–1481.
- H. S. Kim, J. Y. Lee, S. Shin, W. Jeong, S. H. Lee, S. Kim, J. Lee, M. C. Suh and S. Yoo, *Adv. Funct. Mater.*, 2021, **31**, 2104646.
- N. Aizawa, Y. Harabuchi, S. Maeda and Y.-J. Pu, *Nat. Commun.*, 2020, **11**, 3909.
- Y. Xiang, Y. Zhao, N. Xu, S. Gong, F. Ni, K. Wu, J. Luo, G. Xie, Z.-H. Lu and C. Yang, *J. Mater. Chem. C*, 2017, **5**, 12204–12210.
- I. S. Park, H. Min and T. Yasuda, *Angew. Chem., Int. Ed.*, 2022, **61**, e202205684.
- I. S. Park, M. Yang, H. Shibata, N. Amanokura and T. Yasuda, *Adv. Mat.*, 2022, **34**, 2107951.

- 21 M. Nagata, H. Min, E. Watanabe, H. Fukumoto, Y. Mizuhata, N. Tokitoh, T. Agou and T. Yasuda, *Angew. Chem., Int. Ed.*, 2021, **60**, 20280–20285.
- 22 G. L. Eakins, J. S. Alford, B. J. Tiegs, B. E. Breyfogle and C. J. Stearman, *J. Phys. Org. Chem.*, 2011, **24**, 1119–1128.
- 23 T. J. Gately, W. Sontising, C. J. Easley, I. Islam, R. O. Al-Kaysi, G. J. O. Beran and C. J. Bardeen, *CrystEngComm*, 2021, **23**, 5931–5943.
- 24 A. Proń, M. Baumgarten and K. Müllen, *Org. Lett.*, 2010, **12**, 4236–4239.
- 25 W. Li, B. Li, X. Cai, L. Gan, Z. Xu, W. Li, K. Liu, D. Chen and S.-J. Su, *Angew. Chem., Int. Ed.*, 2019, **58**, 11301–11305.
- 26 C. Han, Y. Zhao, H. Xu, J. Chen, Z. Deng, D. Ma, Q. Li and P. Yan, *Chem. – Eur. J.*, 2011, **17**, 5800–5803.
- 27 J. Zhang, D. Ding, Y. Wei and H. Xu, *Chem. Sci.*, 2016, **7**, 2870–2882.
- 28 J. Lee, N. Aizawa, M. Numata, C. Adachi and T. Yasuda, *Adv. Mat.*, 2017, **29**, 1604856.
- 29 S. Oda, B. Kawakami, R. Kawasumi, R. Okita and T. Hatakeyama, *Org. Lett.*, 2019, **21**, 9311–9314.
- 30 K. Masui, H. Nakanotani and C. Adachi, *Org. Electron.*, 2013, **14**, 2721–2726.
- 31 Z. Yang, Z. Mao, Z. Xie, Y. Zhang, S. Liu, J. Zhao, J. Xu, Z. Chi and M. P. Aldred, *Chem. Soc. Rev.*, 2017, **46**, 915–1016.